J|A|C|S
ARTICLES

Published on Web 11/26/2008

Persistence of Camptothecin Analog−Topoisomerase I−DNA Ternary Complexes: A Molecular Dynamics Study

Fung-Ming Siu* and Chi-Ming Che

Department of Chemistry and Open Laboratory of Chemical Biology of the Institute of Molecular Technology for Drug Discovery and Synthesis, The University of Hong Kong, Pokfulam Road, Hong Kong SAR, China

Received September 2, 2008; E-mail: fmsiu@hkucc.hku.hk

Abstract: Topoisomerase I (top1) is the sole chemotherapeutic target for the anticancer alkaloid camptothecin and its analogs (CPTs). The CPTs mediate cytotoxicity by binding reversibly to transient top1−DNA covalent complexes. There is significant variation in the persistence of the resultant CPTs−top1−DNA ternary complexes formed. Presently, there is no reliable method that can be used to predict the persistence of the ternary complexes, significantly limiting formulation of structure−activity relationships. Here, we used molecular dynamics simulations to probe the properties of several CPTs that form ternary complexes of greatly variable persistence. Our study reveals that correlated motions primarily occur between the CPTs and the flanking base pairs. We envision that the nature and strength of the interactions between the CPTs and the flanking base pairs are of key importance and can shed light on the mechanistic basis for the differing persistence of the ternary complexes. Our 'flanking base pairs' models further reveal that the most persistent CPTs (i) have higher calculated free-energy barriers for drug dissociation from the flanking base pairs, (ii) are less sensitive to changes in the rotation angles of the flanking base pairs, (iii) form stronger van der Waals and hydrophobic interactions, and (iv) have larger stacking areas with the flanking base pairs. Collectively, our study demonstrates that molecular dynamics simulations can be used to gain mechanistic insight into the molecular basis for the persistence of the ternary complexes and predict the persistence of such complexes during the drug discovery process.

1. Introduction

Camptothecin (CPT), a potent anticancer drug lead, was isolated from the bark of the Chinese tree *Camptotheca acuminata* about 40 years ago. Topotecan (TPT) and irinotecan are U.S. Food and Drug Administration-approved CPT derivatives for treatment of colon and ovarian cancers.[1] The sole cellular target of CPT and its analogs (CPTs) is type I topoisomerase (top1).[1,2]

Topoisomerases represent molecular targets for a number of anticancer drug leads, and there have been several reviews published on the role of topoisomerases in anticancer drug therapy.[1−3] Relaxation of supercoiled DNA is a key function of top1. DNA relaxation occurs in several steps (Scheme 1a). Top1 clamps around supercoiled DNA. Through a transesterification reaction, the catalytic tyrosine (Tyr723@top1) acts as a nucleophile to cleave one of the DNA strands (nicking, Scheme 1a). Top1 covalently attaches to the 3′-end of the nicked strand to form a transient top1−DNA binary covalent complex. The nick provides a swivel point for DNA rotation. The torsional strain in supercoiled DNA drives the rotation of the 5′-end of the nicked DNA strand around the intact strand (rotation, Scheme 1a). When the 5′-end of the nicked DNA realigns with the corresponding 3′-end, a nick-closing reaction occurs (religation, Scheme 1a). Under normal conditions, the top1−DNA binary covalent complex is transient, as religation is favored over nicking. However, upon binding of the CPTs, the rate of religation is reduced. The CPTs intercalate into the base pairs that flank the cleavage site (nick). Thus, the ends of the cleaved DNA strand in the ternary complex are no longer aligned for efficient religation. Cell killing occurs when the drug-stabilized ternary complex encounters a replication fork, which converts a single DNA strand break into a double DNA strand break (replication fork collision, Scheme 1b). The persistence of the ternary complex increases the likelihood of collision with the replication fork.[4] In other words, CPTs mediate their cytotoxicities by prolonging the lifetime of the ternary complex.[5,6] However, the CPTs-induced ternary complex converts back to the top1−DNA binary complex readily upon drug removal (drug dissociation, Scheme 1b). This limits the clinical applications of CPTs.[7] It has previously been reported that CPTs which bind with greater persistence are more cytotoxic.[4,8,9] Therefore, designing top1 inhibitors that have greater binding persistence

(1) Pommier, Y. *Nat. Rev. Cancer* **2006**, *6*, 789.
(2) Holden, J. A. *Curr. Med. Chem. Anticancer Agents* **2001**, *1*, 1.
(3) Thomas, C. J.; Rahier, N. J.; Hecht, S. M. *Bioorg. Med. Chem.* **2004**, *12*, 1585.
(4) Wang, X.; Wang, L. K.; Kingsbury, W. D.; Johnson, R. K.; Hecht, S. M. *Biochemistry* **1998**, *37*, 9399.
(5) Wang, X.; Zhou, X.; Hecht, S. M. *Biochemistry* **1999**, *38*, 4374.
(6) Champoux, J. J. *Ann. N.Y. Acad. Sci.* **2000**, *922*, 56.
(7) Meng, L. H.; Liao, Z. Y.; Pommier, Y. *Curr. Top. Med. Chem.* **2003**, *3*, 305.
(8) Holden, J. A.; Wall, M. E.; Wani, M. C.; Manikumar, G. *Arch. Biochem. Biophys.* **1999**, *370*, 66.
(9) Tanizawa, A.; Kohn, K. W.; Kohlhagen, G.; Leteurtre, F.; Pommier, Y. *Biochemistry* **1995**, *34*, 7200.

10.1021/ja806934y CCC: $40.75

Scheme 1. (a) Relaxation of Supercoiled DNA by Topoisomerase I; (b) Mode of Action of the CPTs

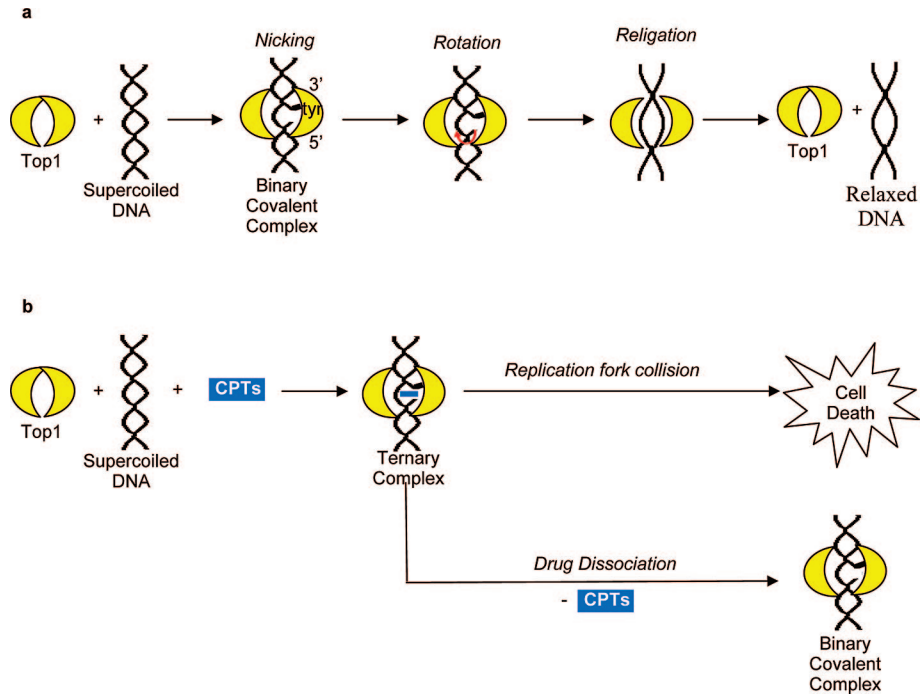

represents an attractive approach for designing more efficacious anticancer agents.[9]

Conversion of CPTs-induced ternary complexes back to binary complexes has been studied in vitro by increasing the concentration of salt (NaCl).[10,11] Pommier and co-workers reported that the half-lives of the ternary complexes under high salt concentration may be related to the persistence of the ternary complexes under physiological conditions.[9] Previously, Holden,[8] Pommier,[9] Hecht,[12,13] and co-workers reported the persistence of various CPTs-induced ternary complexes under high salt conditions. Somewhat surprisingly, the ternary complexes induced by structurally similar CPTs exhibit a significant range of persistence. However, the mechanistic basis of this variation in persistence is not well understood.[12] Correspondingly, it is not possible to predict the persistence of these ternary complexes.

Molecular dynamics (MD) is a well-established method for investigation of structural and dynamic properties of proteins and nucleic acids.[14,15] Previous MD studies successfully revealed the dynamic properties of wild-type and mutated human top1.[16,17] In the present study, we sought to model and rationalize the apparently inexplicable differences in the persistence of various CPTs-induced ternary complexes using MD approaches. From a biomedical perspective, we wanted to gain mechanistic insight into the basis of different persistence with a view to evaluating the potential application of MD approaches for prediction of the persistence of new CPTs-induced ternary complexes.

2. Methods

2.1. Molecular Dynamics Simulation. Crystallographic coordinates were obtained from the Protein Databank (PDB, www.rcsb.org), entry 1K4T.[18] It is generally believed that the lactone form of CPTs can be hydrolyzed to carboxylate form (Supporting Information, Chart S1).[1,2] However, the top1−DNA complex markedly stabilized the lactone form of CPT when compared with the carboxylate form of CPT.[19] The lactone form of CPTs is active against top1, but the carboxylate form is inactive.[1,2] As in previous studies,[19−25] only the active lactone form of CPTs was studied in the present study. The CPTs−top1−DNA ternary complex (Figure 1a) and the CPTs-flanking base pairs (Figure 1b) models are named as ternary complex and flanking base pairs models, respectively. By convention, the nucleotide at the 5′-end of the fragment resulting from top1-mediated cleavage is numbered +1; the one at the 3′-end of the other fragment (covalently linked to top1) is numbered −1. The flanking base pairs models (Figure 1b) include the flanking base pairs (+1, −1) and the CPTs (Chart 1), while all protein residues and the rest of the base pairs are discarded from the 1K4T structure. The 5′-sulfhydryl group is replaced by a 5′-hyroxyl group using Accelrys DS visualizer. The Watson−Crick pairings of the

(10) Champoux, J. J.; Aronoff, R. *J. Biol. Chem.* **1989**, *264*, 1010.
(11) Hsiang, Y. H.; Hertzberg, R.; Hecht, S.; Liu, L. F. *J. Biol. Chem.* **1985**, *260*, 14873.
(12) Cheng, K.; Rahier, N. J.; Eisenhauer, B. M.; Gao, R.; Thomas, S. J.; Hecht, S. M. *J. Am. Chem. Soc.* **2005**, *127*, 838.
(13) Elban, M. A.; Sun, W.; Eisenhauer, B. M.; Gao, R.; Hecht, S. M. *Org. Lett.* **2006**, *8*, 3513.
(14) Cheatham, T. E., III.; Young, M. A. *Biopolymers* **2001**, *56*, 232.
(15) Dixit, S. B.; Beveridge, D. L.; Case, D. A.; Cheatham, T. E., III.; Giudice, E.; Lankas, F.; Lavery, R.; Maddocks, J. H.; Osman, R.; Sklenar, H.; Thayer, K. M.; Varnai, P. *Biophys. J.* **2005**, *89*, 3721.
(16) Fiorani, P.; Bruselles, A.; Falconi, M.; Chillemi, G.; Desider, A.; Benedetti, P. *J. Biol. Chem.* **2003**, *278*, 43268.
(17) Chillemi, G.; Fiorani, P.; Castelli, S.; Bruselles, A.; Benedetti, P.; Desideri, A. *Nucleic Acids Res.* **2005**, *33*, 3339.
(18) Staker, B. L.; Hjerrild, K.; Feese, M. D.; Behnke, C. A.; Burgin, A. B., Jr.; Stewart, L. *Proc. Natl. Acad. Sci. U.S.A.* **2002**, *99*, 15387.
(19) Laco, G. S.; Collins, J. R.; Luke, B. T.; Kroth, H.; Sayer, J. M.; Jerina, D. M.; Pommier, Y. *Biochemistry* **2002**, *41*, 1428.
(20) Xiao, X.; Cushman, M. *J. Am. Chem. Soc.* **2005**, *127*, 9960.
(21) Mazzini, S.; Bellucci, M. C.; Dallavalle, S.; Fraternali, F.; Mondelli, R. *Org. Biomol. Chem.* **2004**, *2*, 505.
(22) Kerrigan, J. E.; Pilch, D. S. *Biochemistry* **2001**, *40*, 9792.
(23) Hansch, C.; Verma, R. P. *ChemMedChem* **2007**, *2*, 1807.
(24) Adams, D. J.; da Silva, M. W.; Flowers, J. L.; Kohlhagen, G.; Pommier, Y.; Colvin, O. M.; Manikumar, G.; Wani, M. C. *Cancer Chemother. Pharmacol.* **2006**, *57*, 135.
(25) Fan, Y.; Weinstein, J. N.; Kohn, K. W.; Shi, L. M.; Pommier, Y. *J. Med. Chem.* **1998**, *41*, 2216.

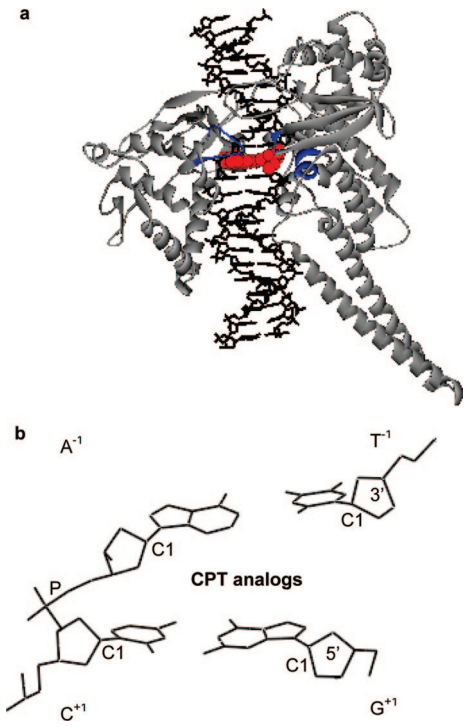

Figure 1. (a) CPTs−top1−DNA ternary complex model: DNA (black, stick), CPT analog (red, CPK), top1 (gray, ribbon), loop 1, loop 2, and loop 3 (blue, ribbon). (b) CPTs-flanking base pairs model.

Chart 1. Structures of the CPTs

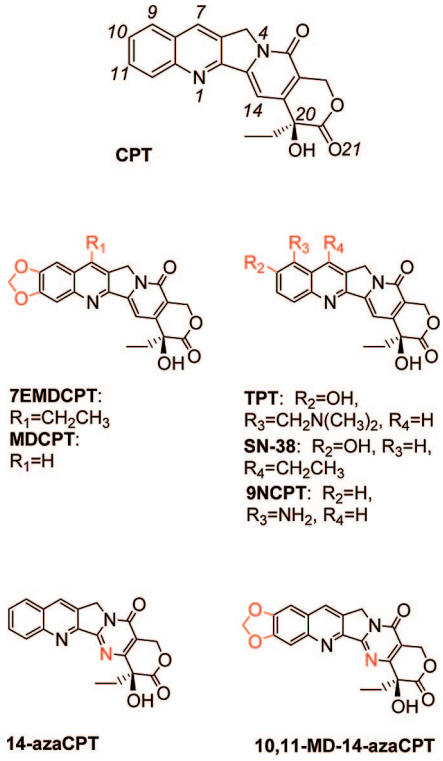

flanking base pairs models were maintained as stated previously.[26] All simulations were performed using the AMBER 8.0 package.[27] Hydrogen atoms were added to the crystallographic structures, and the system topology was built using the AMBER LEAP module.[27] The force field parameters of the CPTs were prepared with the ANTECHAMBER module using the General Amber force field (GAFF).[28] The systems were minimized with the steepest descent algorithm and conjugate gradient method. A generalized Born (GB) model, recently reviewed as capable of rapidly producing stable and reliable trajectories,[29,30] was used to describe the solvated environment. The electrostatic screening effects of salt were incorporated according to experimental conditions via the Debye−Hückel screening parameter.[31] The systems were warmed and equilibrated at 300 K for 200 ps. Production dynamics (3000 ps) were performed at a constant temperature of 300 K using a Langevin thermostat. The simulations remained stable throughout the production period (Supporting Information, Figure S1). The PTRAJ module of AMBER 8.0 was used to analyze saved trajectories.[27] Snapshots were collected for MM-GBSA calculations. The stacking area between the CPTs and the flanking base pairs was calculated by subtracting the solvent-accessible surface area of the CPTs in the presence of the flanking base pairs from the solvent-accessible surface area of the drug alone using Accelrys DS visualizer.[32]

2.2. Dynamic Cross-Correlation Motion. In order to investigate the correlated motion among residues in the ternary complex models, cross-correlation coefficients ($C_{i,j}$) were calculated (eq 1)[27]

$$C_{i,j} = \langle \Delta v_i \Delta v_j \rangle / (\langle \Delta v_i^2 \rangle^{1/2} \langle \Delta v_j^2 \rangle^{1/2}) \quad (1)$$

where Δv_i is the vector displacement from the mean position of residue i, i.e., protein residues (C_α) or DNA bases (N), and Δv_j is the vector displacement from the mean position of residue j, i.e., the CPTs (O_{21}) or the flanking base pairs (N). The angle bracket denotes ensemble average. A positive $C_{i,j}$ indicates that residues i and j move in the same direction; a negative $C_{i,j}$ indicates that the two residues move in opposite directions.

2.3. Potential of Mean Force (PMF). PMF was calculated in order to study the free-energy profiles for the drug dissociation and DNA rotation processes (Scheme 1). PMF was calculated using the molecular simulation package AMBER 8.0.[27]

To mimic the drug dissociation process, PMF as a function of the distance between the CPTs and the flanking base pairs (χ) was calculated (Scheme 2a). The distance (χ) is defined as the distance between P of A^{-1} (Figure 1b) and the midpoint of N1 and N4 of the CPTs (Chart 1). Umbrella sampling was performed by calculating a series of dynamic simulations with biased potential in a format of $K(\chi - \chi_i)^2$, where $K = 10$ kcal mol^{-1}·Å^2 and χ_i ranged from 0 to 40 Å. Each simulation was started from the end point of the previous one, equilibrated for 50 ps and followed by 420 ps of dynamic simulation. Adjacent histograms were found to show significant overlaps, indicating that all values of a distance within the desired range had been appropriately sampled. The unbiased free energy was obtained using the weight histogram analysis method (WHAM)[33] with convergence criterion of 10^{-4} [34] and a bin width of 1 Å.

To mimic the DNA rotation process we calculated PMF along the rotation angle (θ) of the flanking base pairs (Scheme 2b). The rotation angle (θ) is defined as the pseudodihedral angle of the C1 atoms of the flanking base pairs ($\angle T^{-1}-A^{-1}-C^{+1}-G^{+1}$, Figure

(26) Stofer, E.; Chipot, C.; Lavery, R. *J. Am. Chem. Soc.* **1999**, *121*, 9503.
(27) Case, D. A.; Cheatham, T. E., III.; Darden, T.; Gohlke, H.; Luo, R.; Merz, J. K. M.; Onufriev, A.; Simmerling, C.; Wang, B.; Woods, R. J. *J. Comput. Chem.* **2005**, *26*, 1668.
(28) Wang, J.; Wolf, R. M.; Caldwell, J. W.; Kollman, P. A.; Case, D. A. *J. Comput. Chem.* **2004**, *25*, 1157.
(29) Tsui, V.; Case, D. A. *Biopolymers* **2001**, *56*, 275.
(30) Tsui, V.; Case, D. A. *J. Am. Chem. Soc.* **2000**, *122*, 2489.
(31) Srinivasan, J.; Trevathan, M. W.; Beroza, P.; Case, D. A. *Theor. Chem. Acc.* **1999**, *101*, 426.
(32) Staker, B. L.; Feese, M. D.; Cushman, M.; Pommier, Y.; Zembower, D.; Stewart, L.; Burgin, A. B. *J. Med. Chem.* **2005**, *48*, 2336.
(33) Kumar, S.; Bouzida, D.; Swendsen, R. H.; Kollman, P. A.; Rosenberg, J. M. *J. Comput. Chem.* **1992**, *13*, 1011.
(34) Giudice, E.; Várnai, P.; Lavery, R. *Nucleic Acids Res.* **2003**, *31*, 1434.

Scheme 2. Schematic View of the Reaction Coordinates Used in the PMF Calculations: (a) Distance between CPTs and the Flanking Base Pairs (χ, side view of Figure 1b) and (b) Rotation Angle of the Flanking Base Pairs (θ, top view of Figure 1b)

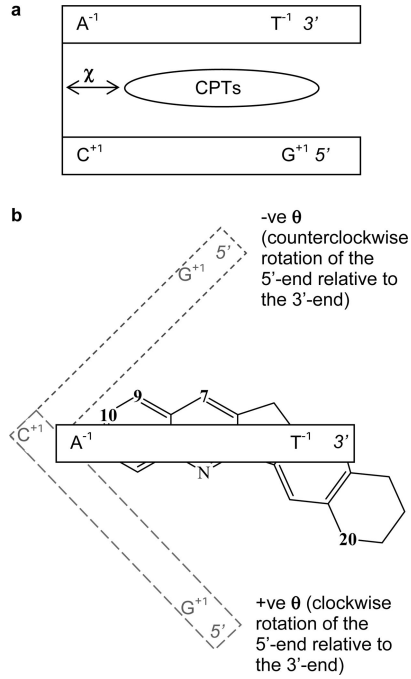

1b), similar to other modeling studies involving base pairs.[35,36] A clockwise rotation of the 5′-end with respect to the intact strand (3′-end) leads to an increase in rotation angle and vice versa for a counterclockwise rotation (Scheme 2b). Using an umbrella sampling technique the system was biased with a harmonic potential $K(\theta - \theta_i)^2$ centered on successive values of rotation angle (θ_i) ranging from −100° to 100°. Harmonic force constants (K) of 30 or 10 kcal mol^{-1} rad^{-2} were used. For each window the MD simulation consisted of 50 ps equilibration and 420 ps sampling. The conformation obtained at the end of this sampling was used as the starting point for the following window. It was verified that adjacent histograms showed significant overlaps, indicating that all values of angles within the specified range were appropriately sampled. The PMF was obtained using WHAM[33] with a bin width of 2° and tolerance of 10^{-4}.[34]

2.4. Molecular Mechanics-Generalized Born Surface Area (MM-GBSA). The binding energies were obtained using a post-processing method, MM-GBSA scripts supplied with AMBER 8.0.[27] MM-GBSA has been known to be good at qualitative accuracy.[37]

The total binding energy (ΔG_{tot}) was decomposed into contributions from electrostatic energies (ΔE_{elec}), van der Waals (ΔE_{vdw}), electrostatic solvation free energies (ΔG_{GB}), nonpolar solvation ($\Delta G_{nonpolar}$), and entropy (TS) as shown in eq 2

$$\Delta G_{tot} = \Delta E_{elec} + \Delta E_{vdw} + \Delta G_{GB} + \Delta G_{nonpolar} - TS \quad (2)$$

$$\text{electrostatic components} = \Delta E_{elec} + \Delta G_{GB} \quad (3)$$

$$\text{nonpolar components} = \Delta E_{vdw} + \Delta G_{nonpolar} \quad (4)$$

The energies of electrostatic (ΔE_{elec}) and van der Waals (ΔE_{vdw}) interactions were calculated using molecular mechanics with an empirical force field. The solvation free energy was estimated from the electrostatic solvation energy (ΔG_{GB}) and the nonpolar solvation energy ($\Delta G_{nonpolar}$). The contributions from electrostatic and nonpolar interactions are classified in eqs 3 and 4, respectively. A generalized Born (GB) model was used to estimate the electrostatic solvation energy (ΔG_{GB}). Nonpolar solvation energies ($\Delta G_{nonopolar}$) were determined by solvent-accessible surface area (SASA) dependent terms (eq 5) computed using the MOLSURF program with $\gamma = 0.00542$ kcal Å^{-1} and $\beta = 0.92$ kcal mol^{-1}.

$$\Delta G_{nonpolar} = \gamma(\text{SASA}) + \beta \quad (5)$$

In the original MM-GBSA formalism entropic contributions (TS, eq 2) were calculated based on classical statistical formulas and normal-mode analysis. However, the uncertainty in the calculation of the entropic components to the free energy is yet to be resolved. It is generally believed that entropy prediction has a significant systematic error, considering that the normal-mode analysis is based on a harmonic approximation.[37−40] As our primary goal was merely to calculate the relative binding energies of a series of similarly sized molecules binding to a common binding site, the entropic contribution was omitted, as has been the case in previous studies.[41,42]

Table 1. Half-Lives of the CPTs−top1−DNA Ternary Complexes

CPTs[a]	half-life (min)[b]	half-life (min)[c]	rate constant ($\times 10^{-3}$ s^{-1})[d]	rate constant ($\times 10^{-3}$ s^{-1})[e]
7EMDCPT	42			
MDCPT	11	1.3		
SN-38	11	0.9		
TPT	4	0.5		
9NCPT	1.5	0.4		
CPT	1	0.3	18.3	
10,11-MD-14-azaCPT				21.5
14-azaCPT			115	115

[a] 7EMDCPT = 7-ethyl-10,11-methylenedoxy-camptothecin; MDCPT = 10,11-methylenedoxy-camptothecin; SN-38 = 7-ethyl-10-hydroxy-camptothecin; TPT = topotecan; 9NCPT = 9-aminocamptothecin; CPT = camptothecin; 10,11-MD-14-azaCPT = 10,11-methylenedoxy-campto thecin; 14-azaCPT = 14-azacamptothecin. [b] Experiment (0.45 M NaCl) performed by Holden et al.[8] [c] Experiment (0.35 M NaCl) performed by Tanizawa et al.[9] [d] Experiment (0.35 M NaCl) performed by Cheng et al.[12] [e] Experiment (0.35 M NaCl) performed by Elban et al.[13]

3. Results and Discussion

3.1. Molecular Dynamics Simulation of the CPTs−top1−DNA Ternary Complexes. The differing persistence of several CPTs-induced ternary complexes was reported by Holden,[8] Tanizawa,[9] Cheng,[12] Elban,[13] and co-workers (Table 1). For instance, Holden et al. reported that by incorporating the 7-ethyl and 10,11-methylendioxy moieties to CPT (Chart 1), the half-life of the 7-ethyl-10,11-methylenedioxy-camptothecin (7EMDCPT)-induced ternary complex was 42 times longer than that of CPT (Table 1).[8] Cheng et al. reported that the off-rate of 14-azacamptothecin (14-azaCPT) was ∼6 times faster than that of CPT (Table 1).[12] However, 14-azaCPT and CPT are structurally similar (Chart 1), differing only at position 14, with an N atom (14-azaCPT) in lieu of the CH (CPT). 7EMDCPT-

(35) O'Neil, L. L.; Grossfield, A.; Wiest, O. *J. Phys. Chem. B* **2007**, *111*, 11843.
(36) Bernet, J.; Zakrzewska, K.; Lavery, R. *J. Mol. Struct. (Theochem)* **1997**, *398−399*, 473.
(37) Rizzo, R. C.; Toba, S.; Kuntz, I. D. *J. Med. Chem.* **2004**, *47*, 3065.
(38) Srinivasan, J.; Cheatham, T. E., III.; Cieplak, P.; Kollman, P. A.; Case, D. A. *J. Am. Chem. Soc.* **1998**, *120*, 9401.
(39) Wang, J.; Morin, P.; Wang, W.; Kollman, P. A. *J. Am. Chem. Soc.* **2001**, *123*, 5221.
(40) Tsui, V.; Case, D. A. *J. Phys. Chem. B* **2001**, *105*, 11314.
(41) Kollman, P. A.; Massova, I.; Reyes, C.; Kuhn, B.; Huo, S.; Chong, L.; Lee, M.; Lee, T.; Duan, Y.; Wang, W.; Donini, O.; Cieplak, P.; Srinivasan, J.; Case, D. A.; Cheatham, T. E., III. *Acc. Chem. Res.* **2000**, *33*, 889.
(42) Wu, C.; Wang, Z.; Lei, H.; Zhang, W.; Duan, Y. *J. Am. Chem. Soc.* **2007**, *129*, 1225.

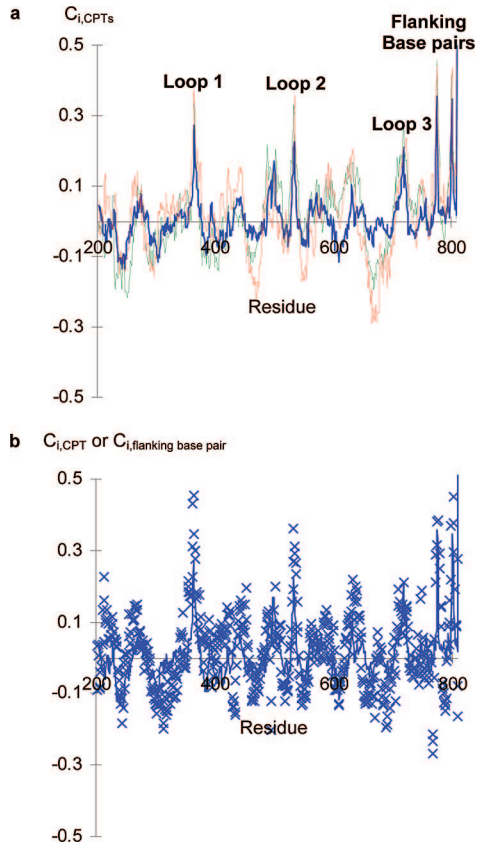

Figure 2. (a) Dynamic cross-correlation against the CPTs ($C_{i,CPTs}$, line) for the 7EMDCPT (green), CPT (blue), and 14-azaCPT (red) bound ternary complexes. Those regions with higher $C_{i,CPTs}$ are labeled. (b) Dynamic cross-correlation against the CPT ($C_{i,CPT}$, line) or the flanking base pairs (Ci,flanking base pairs, cross) for the CPT-induced ternary complex.

and 14-azaCPT-induced ternary complexes represent the most and least persistent ternary complexes studied in the present study.

Molecular dynamics simulations of the 7EMDCPT (most persistent), CPT (parent structure), and 14-azaCPT (least persistent) bound top1−DNA ternary complexes were performed in order to evaluate the dynamic properties of these three ternary complexes, which have significantly different persistence. The structure of a ternary complex is shown in Figure 1a.

3.1.1. Dynamic Cross-Correlation Motions. Dynamic cross-correlation analyses were performed to reveal the correlated motions between the CPTs and DNA/protein residues in the ternary complexes. Among the DNA residues (residues 766 to 809), the flanking base pairs had the highest positive dynamic cross-correlation coefficient ($C_{i,CPTs}$) values (~0.5, Figure 2a), implying that correlated motions between these CPTs and the flanking base pairs do occur. For the protein residues (residues 200 to 765), loop 1 (Phe361 to Lys369, Figure 1a), loop 2 (Lys532 to Ser534, Figure 1a), and loop 3 (Thr718 to Tyr723, Figure 1a) had relatively higher $C_{i,CPTs}$ values (~0.4, Figure 2a). Consistent with a review published by Pommier et al.,[43] single mutations (residues Phe361, Arg362, Gly363, Arg364, Asp533, and Asn722) in top1 that confer CPT resistance is mainly localized in these three loops.

Pommier and co-workers reported that CPTs form similar hydrogen bonds with protein residues in the ternary complexes.[44] In the X-ray structure of a TPT-induced ternary complex there is one direct hydrogen bond between top1 and TPT.[18] Xiao and Cushman reported that the hydrogen bonding of CPT to the surrounding amino acid residues of top1 is of minor significance in predicting the binding orientation and DNA sequence selectivity of CPT.[20] The X-ray crystal structures of the CPTs-induced ternary complexes revealed that the contact areas between CPTs and protein residues are small.[18,32] Collectively, the correlated motions between the CPTs and the protein residues may not be attributable to direct interactions.

The majority of the solvent-accessible surface area of the CPTs is covered by base-stacking interactions as revealed in the X-ray crystal structures of the CPTs-induced ternary complexes.[18,32] A previous dynamic cross-correlation analysis on a top1−DNA binary complex revealed correlated motions between Gly363/Arg364 (loop 1) and the −1 base of the intact strand.[45] It is conceivable that the correlated motions between the CPTs and the protein residues are mediated by the flanking base pairs rather than through direct interactions. The results of dynamic cross-correlation analysis between the flanking base pairs and the protein residues in the CPT−top1−DNA ternary complex are shown in Figure 2b. As expected, the correlated motions between the flanking base pairs and the protein residues are similar or even stronger than those between the CPT and the protein residues (i.e., $C_{i,flanking\ base\ pairs} \geq C_{i,CPT}$, Figure 2b). Similar results were observed for the cases of the 7EMDCPT/14-azaCPT-induced ternary complexes. These findings imply that the primary correlated motions occur between the CPTs and the flanking base pairs. These primary correlated motions affect the protein residues localized in loop 1, loop 2, and loop 3. Extensive hydrogen bonding between the flanking base pairs and the protein residues ($A^{-1}\cdots$Arg364, $C^{+1}\cdots$Arg364, $T^{-1}\cdots$Lys443, $G^{+1}\cdots$Asn722, and $T^{-1}\cdots$P-Tyr723) were observed in the present molecular dynamics simulations study. The correlated motions between the flanking base pairs and the protein residues may be mediated through a hydrogen-bonding network. The X-ray crystal structure of a TPT-induced ternary complex revealed that the intercalation binding site is created by conformational changes within the flanking base pairs, which are stabilized through a hydrogen-bonding network with the protein residues.[18] The positioning of the uncleaved strand is stabilized through hydrogen-bond contacts to Arg362 and Gly363 residues. Thr718, Arg364, and Lys532 form hydrogen bonds with G^{+1}, A^{-1}, and T^{-1}, respectively.[18] Collectively, these findings imply that the correlated motions occur between the CPTs and the flanking base pairs, which communicate with the neighboring protein residues. We speculate that the nature and strength of the primary interactions between the CPTs and the flanking base pairs are important factors underlying the significant differences in the persistence of the ternary complexes.

3.2. Flanking Base Pairs Models. Holden et al. measured the half-lives of six different CPTs-induced ternary complexes (Table 1).[8] The six CPTs studied were 7EMDCPT, MDCPT (10,11-methylenedoxy-camptothecin), SN-38 (7-ethyl-10-hydroxycamptothecin), TPT, 9NCPT (9-aminocamptothecin), and CPT. The half-lives for five of these CPTs-induced ternary

(43) Pommier, Y.; Pourquier, P.; Urasaki, Y.; Wu, J.; Laco, G. S. *Drug Resist. Updates* **1999**, *2*, 307.
(44) Marchand, C.; Antony, S.; Kohn, K. W.; Cushman, M.; Ioanoviciu, A.; Staker, B. L.; Burgin, A. B.; Stewart, L.; Pommier, Y. *Mol. Cancer Ther.* **2006**, *5*, 287.
(45) Chillemi, G.; Fiorani, P.; Benedetti, P.; Desideri, A. *Nucleic Acids Res.* **2003**, *31*, 1525.

complexes were also reported by Tanizawa et al. (Table 1).[9] These two sets of data are in qualitative agreement with a correlation coefficient of 0.9 (Supporting Information, Figure S2). For consistency and simplicity, only the data of Holden et al. are discussed in the following sections. In our 'flanking base pairs' models the interactions between the CPTs (Chart 1) and the flanking base pairs (Figure 1b) were studied. We note that the interactions between DNA and various CPTs have previously been reported.[21,46] However, these studies are quite different from the one reported here as they involved intact DNA. As a result, these CPTs can only bind to the end of the double helix,[21,46] but cannot intercalate with DNA, as is the case for the ternary complexes. In fact, the intercalation binding pocket in the ternary complexes can form only after trans-esterification (with tyrosine723 of top1) has occurred, which effectively 'opens-up' the backbone of one strand of the duplex, creating a space for intercalation. We envision that the flanking base pairs models reveal the intrinsic properties of the binding between the flanking base pairs and the CPTs. This is more biologically relevant for the following reasons: (i) the effect of the neighboring residues (protein and other DNA base pairs) is discarded; (ii) a nick is introduced between A-T and C-G base pairs (Figure 1b), which is commonly considered to be a preferred intercalation site for the CPTs; and (iii) a native hydroxyl group at the 5′-end of the nicked strand is used.

3.2.1. Potential of Mean Force (Distance). Dissociation of the CPTs from the ternary complexes affects the persistence of the ternary complexes (drug dissociation, Scheme 1b).[4] The potential of mean force (PMF) is defined as the free-energy changes along an arbitrarily defined path. To study the dissociation process, one of the most obvious pathways is to simply pull out the CPTs from the intercalation site of the flanking base pairs (Scheme 2a). The reaction coordinate is defined as the distance between the CPTs and the flanking base pairs (χ). The location of the unbound state was determined to be where the PMF flattened out.[47] The PMFs of the 7EMDCPT-flanking base pairs models were found not to depend significantly on cutoff value, bin size, or sampling time per window (Supporting Information, Figure S3). Thus, the simulations were considered to have converged.

The PMFs of various flanking base pairs models are shown in Figure 3. The minima ($\chi \approx 11$ Å) correspond to a region of the path with extensive stacking interactions. When the PMF of 7EMDCPT-flanking base pairs model (most persistent) was compared with that of CPT-flanking base pair model (least persistent), two differences were observed. First, the free energy peaks at 26 Å in the 7EMDCPT-flanking base pairs model. In the CPT-flanking base pairs model the free energy flattens out at 23 Å. In general, one would expect the free energy to flatten out when the corresponding CPTs-flanking base pairs interaction energy decays to zero. The longer plateau distance in the case of 7EMDCPT may be attributed to binding of the additional methylenedioxy moiety with the flanking base pairs. Second, the free-energy barrier (ΔG_{PMF}) of the 7EMDCPT-flanking base pairs model (11 kcal mol^{-1}) is remarkably higher than that of the CPT-flanking base pairs model (8 kcal mol^{-1}). From the PMFs calculated under various conditions (Supporting Information, Figure S3), the statistical error[26] of the calculated free-energy barriers was found to be 0.2 kcal mol^{-1}. This suggests

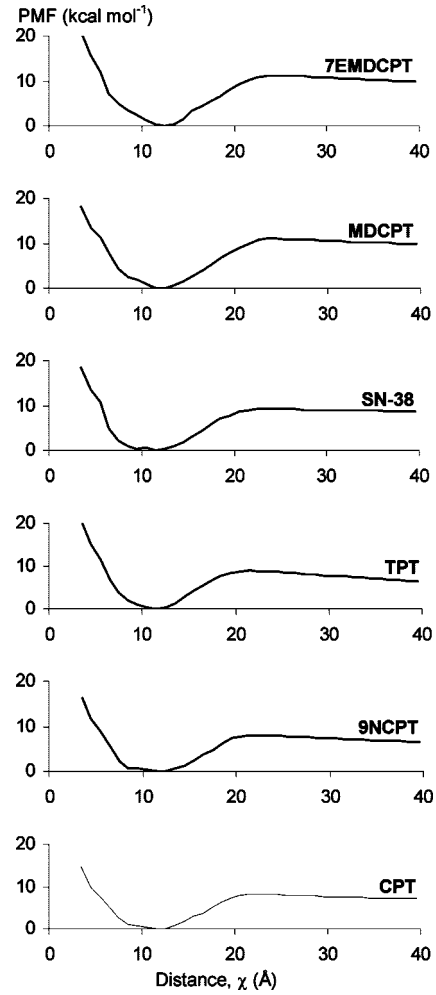

Figure 3. PMFs of the CPTs-flanking base pairs models as a function of distance (χ).

that 7EMDCPT dissociates less readily from the flanking base pairs when compared with CPT.

For qualitative comparisons, the experimental half-lives of the ternary complexes listed in Table 1 were converted to off-rates following first-order kinetics,[4,8] i.e., off-rate = ln(2)/half-life. On the basis of transition-state theory, the free-energy barriers for dissociation of the CPTs from the ternary complexes (ΔG_{TC}) were calculated using eq 6[48−50]

$$\text{off-rate} = \kappa \frac{k_B T}{h} \exp\left(\frac{-\Delta G_{TC}}{RT}\right) \tag{6}$$

where k_B, h, and R are the Boltzmann's, Planck's, and gas constants, respectively. The ΔG_{TC} is the free-energy barrier, and T is the absolute temperature. The transmission constant (κ) was assumed to be unity. According to transition-state theory the free-energy barriers for dissociation of CPTs from the ternary complexes (ΔG_{TC}) were estimated to be on average 21 kcal mol^{-1}. We would like to emphasize that the calculated free-energy barriers shown in the PMFs of Figure 3 (ΔG_{PMF}) cannot quantitatively represent the ΔG_{TC} determined from the ternary complexes (Table 1) for the following reasons. Theoretically,

(46) Bocian, W.; Kawecki, R.; Bednarek, E.; Sitkowski, J.; Pietrzyk, A.; Williamson, M. P.; Hansen, P. E.; Kozerski, L. *Chem. Eur. J.* **2004**, *10*, 5776.
(47) Lee, M. S.; Olson, M. A. *Biophys. J.* **2006**, *90*, 864.
(48) Agarwal, P. K.; Billeter, S. R.; Hammes-Schiffer, S. *J. Phys. Chem. B* **2002**, *106*, 3283.
(49) Lazaridis, T.; Paulaitis, M. E. *J. Am. Chem. Soc.* **1994**, *116*, 1546.
(50) Wu, J.; Xu, D.; Lu, X.; Wang, C.; Guo, H.; Dunaway-Mariano, D. *Biochemistry* **2006**, *45*, 102.

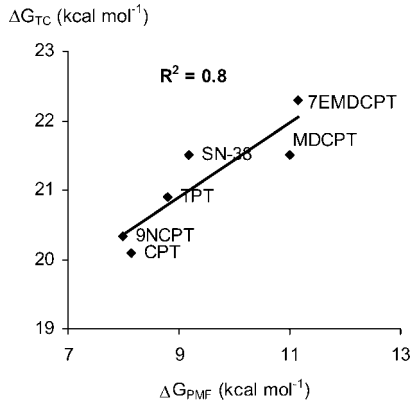

Figure 4. Correlation between experimental free-energy barriers for dissociation of the CPTs from the top1−DNA ternary complexes (ΔG_{TC}) and calculated free-energy barriers for dissociation of the CPTs from the flanking base pairs calculated by potential of mean force approach (ΔG_{PMF}).

the transmission constant (κ) may be less than unity. Thus, ΔG_{TC} (calculated based on eq 6) represents an upper bound to the true barrier.[51] Physically, the cleavage site is clamped by protein residues in the ternary complexes. Thus, drug dissociation from the ternary complex may be hindered by the protein residues. As a result, the experimental ΔG_{TC} determined from the ternary complexes should be quantitatively higher than the theoretical ΔG_{PMF} calculated from the PMFs of the flanking base pairs models. Nevertheless, ΔG_{PMF} correlated with ΔG_{TC} qualitatively. As shown in Figure 4, a positive correlation between ΔG_{PMF} and ΔG_{TC} was obtained ($R^2 = 0.8$). Logically, free-energy barriers for dissociation of the less persistent CPTs from the flanking base pairs are lower. In other words, ΔG_{PMF} represents the free-energy barrier for dissociation of the less persistent CPTs from the flanking base pairs, which correlates with the persistence of the CPTs-induced ternary complexes.

3.2.2. Potential of Mean Force (Rotation Angle). During DNA relaxation, torsional energy within the positive/negative supercoiled DNA drives the clockwise/counterclockwise rotation of the nicked strand around the intact strand at the cleavage site (rotation, Scheme 1a). A recent single-molecule nanomanipulation study of a TPT-induced ternary complex showed that slow and continuous uncoiling of the supercoiled DNA occurred in the presence of TPT.[52] When the cleaved strand passes the intact DNA strand during DNA rotation the rotation angle of the flanking base pairs changes significantly (Scheme 2b). This process may have a large impact on the interaction between the CPTs and the flanking base pairs. To ascertain the energetic consequences of the DNA rotation during DNA relaxation we studied the PMF characterizing the rotation angle of the flanking base pairs (Scheme 2b). The PMFs of the 7EMDCPT-flanking base pairs models did not depend significantly on cutoff value, bin size, or sampling time per window (Supporting Information, Figure S4). Thus, the simulations were considered to have converged.

The PMF of 7EMDCPT shows two distinct regions: a quadratic zone and a roughly linear zone (Figure 5). The minimum corresponds to the best stacking complexes. For the quadratic zone ($-20° <$ rotation angle (θ) $< 50°$, gray rectangle, Figure 5), the free energy increases quadratically. The standard derivation[26] of the ranges of the quadratic zone determined from

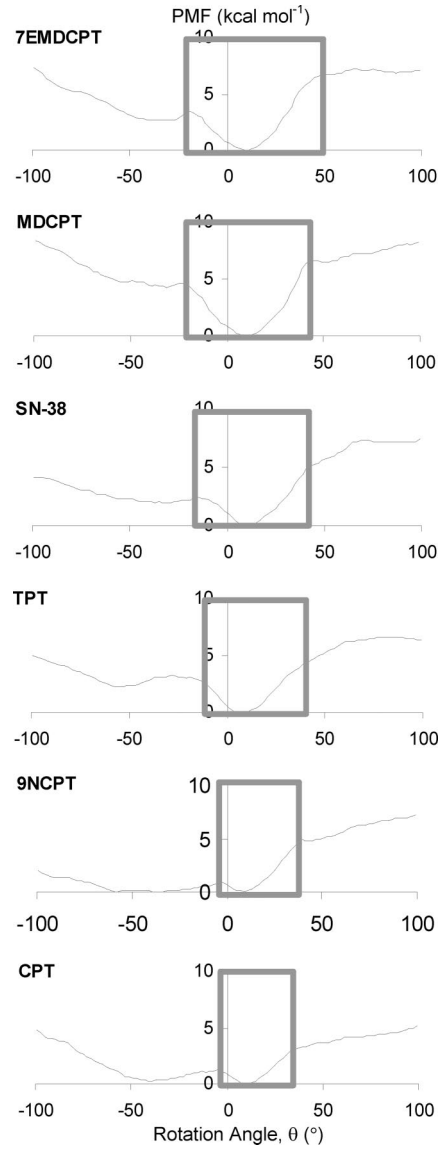

Figure 5. PMFs of the CPts-flanking base pairs models as a function of rotation angle (θ).

the PMFs calculated under various conditions (gray rectangle, Supporting Information, Figure S4) was found to be less than 2°. In the linear zone, the increase in free energy is less dramatic. Finally, the free energies flatten out at roughly 7 and 4 kcal mol^{-1}, respectively, for the positive ($\theta > 0$) and negative ($\theta < 0$) sides (Figure 5). The initial quadratic rise in free energy corresponds to weakening of stacking interactions. The 7EMDCPT still intercalates (fully/partly) into the flanking base pairs when the rotation angle changes from $-20°$ to 50°. Below $-20°$ or above 50° the stacking interaction is no longer maintained. Consequently, 7EMDCPT and the flanking base pairs are free to look for stabilizing interactions with their neighbors. The flanking base pairs form transient hydrogen bonds with 7EMDCPT.

The ranges of the quadratic zone (gray rectangle, Figure 5) correspond to the ranges of the rotation angle that permit favorable intercalation of the CPTs into the flanking base pairs. We note that the ranges of the quadratic zone decreased with the order 7EMDCPT > MDCPT > SN-38 > TPT > 9NCPT > CPT. This order is in qualitative agreement with the reported experimental off-rates determined for the ternary complexes

(51) Kottalam, J.; Case, D. A. *J. Am. Chem. Soc.* **1988**, *110*, 7690.
(52) Koster, D. A.; Palle, K.; Bot, E. S. M.; Bjornsti, M. A.; Dekker, N. H. *Nature* **2007**, *448*, 213.

Table 2. Calculated Total Energies and Their Components (kcal mol^{-1}) of the Flanking Base Pairs Models;[a] Correlation Coefficients (R^2) between Experimental off-rates of Dissociation of the CPTs from the Ternary Complexes and the Calculated Energies

	ΔE_{elec}	ΔE_{vdw}	ΔG_{GB}	$\Delta G_{nonpolar}$	electrostatic components ($\Delta G_{GB}+\Delta E_{elec}$)	nonpolar components ($\Delta G_{nonpolar}+\Delta E_{vdw}$)	ΔG_{tot}
7EMDCPT	−3	−46	21	−3	18	−49	−31
SN-38	−5	−46	24	−3	20	−49	−29
MDCPT	−4	−45	21	−3	17	−47	−30
TPT	−5	−44	24	−3	19	−47	−28
9NCPT	−4	−42	21	−3	17	−45	−27
CPT	−1	−40	18	−3	17	−43	−26
R^2	0.5	0.9	0.5	0.3	0.4	0.9	0.8

[a] The standard error of mean <0.5 kcal mol^{-1}.

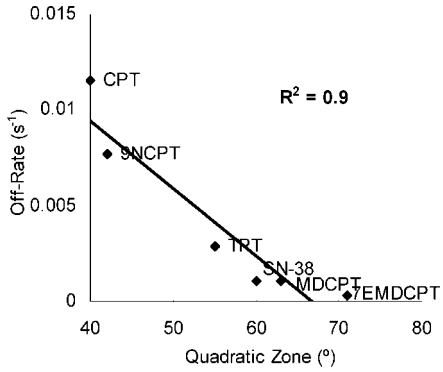

Figure 6. Correlation between off-rates determined for dissociation of the CPTs from the top1−DNA ternary complexes and range of quadratic zone.

(converted from the half-lives shown in Table 1). A negative correlation between the off-rates and the ranges of the quadratic zone was obtained ($R^2 = 0.9$, Figure 6). This indicates that the CPTs that are able to induce persistent ternary complexes are less sensitive to changes in the rotation angles, but the less persistent CPTs (9NCPT and CPT) are more sensitive. Correspondingly, the CPTs that are able to induce persistent ternary complexes would be expected to be more highly retained in the cleavage site during rotation of the two DNA strands (i.e., with large variations in rotation angle).

Our flanking base pairs models provide intrinsic insight into how the chemical structures of CPTs affect the rotation of the flanking base pairs. For top1 the torque forces involved in the DNA rotation process are expected to be asymmetric during coiling or uncoiling.[53] Therefore, it is not surprising to note that the PMFs shown in Figure 5 are also asymmetric. For the positive side, similar free-energy barriers were observed (Figure 5). This may be attributed to the fact that all the CPTs studied here have an ethyl group at position 20, which hinders clockwise rotation of the 5′-end of the cleaved DNA strand (relative to the 3′-end) to a similar extent in each case (Scheme 2b). However, for the negative side, large discrepancies were observed (Figure 5). For 7EMDCPT, MDCPT, SN-38, and TPT the effective stacking and bulky groups at positions 7, 9, 10, and 11 make the counterclockwise rotation of the 5′-end (relative to the 3′-end) difficult (Scheme 2b). On the other hand, the amino group at position 9 of 9NCPT is relatively small. Thus, the free-energy barriers for counterclockwise rotation (negative side) are lower in the 9NCPT and CPT (no side chain)-flanking base pairs models. We note that the published experimental results on how CPTs impair supercoil relaxation by top1 remain contradictory. CPT was found to inhibit a bovine liver mitochondria top1 from relaxing positive and negative supercoils. However, removal of negative supercoils was more severely impaired by drug administration than removal of positive supercoils (60-fold differences).[54] For wild-type human top1 Knudsen and co-workers reported that the inhibition effects of CPT on positive supercoil relaxation (40- to 60-fold) were less pronounced than those found for negative supercoil relaxation (150-fold).[55] However, these results contradict recently published data obtained by single DNA molecule and in vivo investigations.[52] In the work by Koster et al., TPT was found to hindered DNA uncoiling with a more pronounced effect on removal of positive versus negative supercoils.[52] Clearly, additional experiments are necessary to elucidate the reasons underlying these discrepancies. We would like to emphasize that the flanking base pairs models reported here cannot be used to explain these discrepancies. This is because our flanking base pairs models do not take the "controlled rotation" of DNA into consideration. According to the "controlled rotation" mechanism of human top1 as suggested by Champoux and co-workers DNA relaxation proceeds by rotation of the free 5′-end around the intact strand in a manner that is restricted by the surrounding protein.[56] Nevertheless, our results imply that the CPTs intrinsically impair supercoil relaxation in an asymmetric manner: a prediction borne out by our calculations.

3.2.3. MM-GBSA. To gain further insight into the origin of persistence of ternary complexes we used MM-GBSA to calculate binding energies for the flanking base pairs. The total binding energies and their components are listed in Table 2. The total binding energies range from −26 to −31 kcal mol^{-1} (Table 2). We consider these values to be reasonable as Song et al. recently reported that the ab initio binding energy of a norindenoisoquinoline (top1 inhibitor) to simplified DNA base pairs is −32 kcal mol^{-1}.[57]

As highlighted in Table 2, the major favorable contributor to binding is the van der Waals interaction energy (ΔE_{vdw}). Similar to the findings reported in previous studies,[37,39,42] the electrostatic solvation energy (ΔG_{GB}) term opposes binding (Table 2). The electrostatic interactions between the CPTs and the flanking base pairs may be quite strong, but the electrostatic interactions between the CPTs and solvent are much stronger. Thus, when the CPTs transfer from the solvent to the binding pocket, the electrostatic contributions for CPTs are unfavorable

(53) Marko, J. F. *Phys. Rev. E* **2007**, *76*, 021926.
(54) Lin, J. H.; Castora, F. J. *Arch. Biochem. Biophys.* **1995**, *324*, 293.
(55) Frøhlich, R. F.; Veigaard, C.; Andersen, F. F.; McClendon, A. K.; Gentry, A. C.; Andersen, A. H.; Osheroff, N.; Stevnsner, T.; Knudsen, B. R. *Nucleic Acids Res.* **2007**, *35*, 6170.
(56) Stewart, L.; Redinbo, M. R.; Qiu, X.; Hol, W. G. J.; Champoux, J. J. *Science* **1998**, *279*, 1534.
(57) Song, Y.; Cushman, M. *J. Phys. Chem. B* **2008**, *112*, 9484.

to the binding.[58] Nonpolar components ($\Delta G_{nonpolar} + \Delta E_{vdw}$) are the main favorable contributors to the total binding energy (ΔG_{tot}) rather than the electrostatic components ($\Delta G_{GB} + \Delta E_{ele}$). The standard errors of the mean for these energies were found to be less than 0.5 kcal mol^{-1}.[37] Our finding is in accordance with the results of Laco et al., who studied SN-38/CPT-bound ternary complexes.[19] Laco et al. divided the total interaction energies of these complexes into van der Waals and electrostatic interactions, with the former found to be the dominant factor.[19] In contrast with our findings, Xiao et al. found that electrostatic interactions between indenoisoquinolines (top1 inhibitor) and the flanking base pairs played the major stabilizing role.[59] This discrepancy may be attributed to the effect of salt. Salt may screen out electrostatic interactions. In Xiao et al.'s study electrostatic potential surface maps were calculated in the absence of salt. In the MD simulations described here high salt conditions were used to mimic experimental conditions required for the off-rates measurements.

In order to probe factors underpinned the persistence of the ternary complexes we sought to identify whether there are any correlations between the individual energy terms and the off-rates (converted from the half-lives shown in Table 1). The correlation coefficients are shown in Table 2 and Figure 7. A poor correlation between the off-rates and the electrostatic components ($\Delta G_{GB} + \Delta E_{elec}$, $R^2 = 0.4$) is depicted in Figure 7a. However, a strong correlation between the off-rates and the nonpolar components ($\Delta G_{nonpolar} + \Delta E_{vdw}$, $R^2 = 0.9$, Figure 7b) was observed. As nonpolar components are the dominant factors and compensate with the electrostatic components, their sum (ΔG_{tot}) have an R^2 of 0.8 (Figure 7c). This result implies that nonpolar interactions between the CPTs and the flanking base pairs may be a major factor underlying the persistence of the ternary complexes. This speculation is in accordance with reports in the literature. Tanizawa et al. suggested that hydrophobic moieties on the CPTs may increase their binding affinity to the cleavage site.[9] A recent quantitative structure−activity relationship study has revealed that the inhibitory activity of CPTs toward top1 is mainly dependent on hydrophobic descriptors.[23]

In general, nonpolar interactions become stronger as the contact area increases. We speculate that the off-rates may also correlate with the stacking areas between the CPTs and the flanking base pairs. As expected, the off-rates decrease as the stacking areas increase with an R^2 of 0.8 (Figure 8). To further verify our findings the X-ray crystal structures of TPT and CPT-bound tertiary complexes were compared. The TPT-induced ternary complex is more persistent than that of CPT. In literature, the solvent-accessible surface area of TPT covered by DNA (390 Å^2; PDB: 1K4T) was reported to be larger than that of CPT (378 Å^2; PDB: 1T8I).[32]

For the sake of qualitative comparison, we also performed MM-GBSA analyses for the 7EMDCPT/CPT−top1−DNA ternary complexes (Table 3). In accordance with the deduction derived from our flanking base pairs models, the MM-GBSA analyses of the ternary complexes also revealed that nonpolar components ($\Delta G_{nonpolar} + \Delta E_{vdw}$) are the dominant factor when compared with the electrostatic components ($\Delta G_{GB} + \Delta E_{elec}$). In addition, the energies of the nonpolar components ($\Delta G_{nonpolar} + \Delta E_{vdw}$) for the persistent analog (7EMDCPT) are higher than those of the less persistent analog (CPT). As only qualitative trends are discussed here, we conclude the flanking base pairs models could be used to gain mechanistic insight with a lower computational cost.

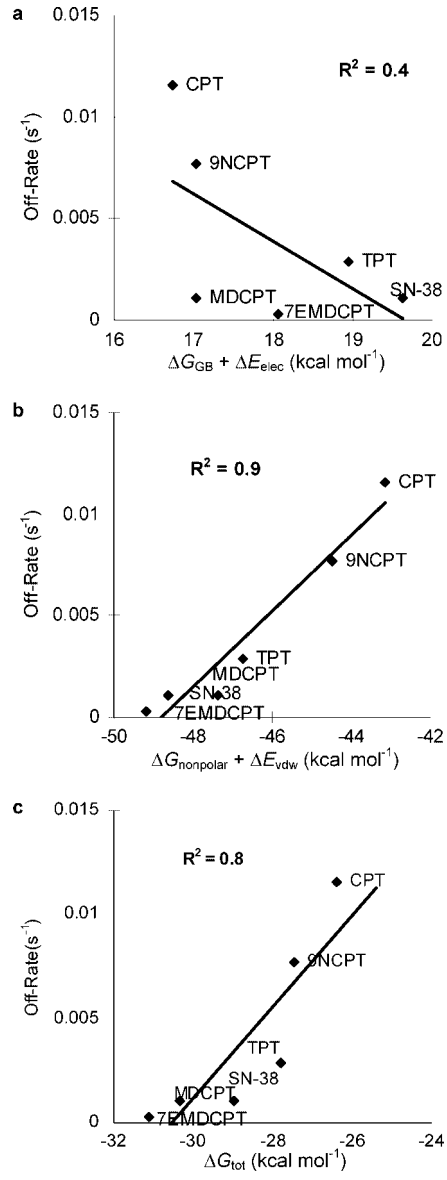

Figure 7. Correlation between off-rates determined for dissociation of the CPTs from the top1−DNA ternary complexes and calculated energies: (a) electrostatic components ($\Delta G_{GB} + \Delta E_{elec}$), (b) nonpolar components ($\Delta G_{nonpolar} + \Delta G_{vdw}$), and (c) total binding energy (ΔG_{tot}).

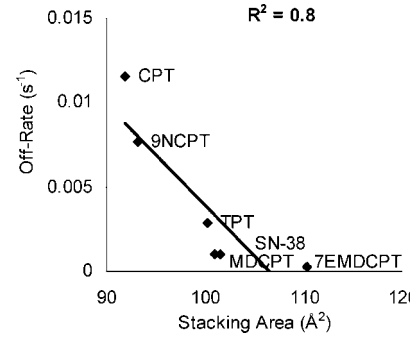

Figure 8. Correlation between off-rates determined for dissociation of the CPTs from the top1−DNA ternary complexes and stacking area between the CPTs and the flanking base pairs.

(58) Yan, C.; Xiu, Z.; Li, X.; Li, S.; Hao, C.; Teng, H. *Proteins* **2008**, *73*, 134.
(59) Xiao, X.; Antony, S.; Pommier, Y.; Cushman, M. *J. Med. Chem.* **2005**, *48*, 3231.

Table 3. Calculated Total Energies and Their Components (kcal mol^{-1}) of the CPTs−top1−DNA Ternary Complex Models[a]

	ΔE_{elec}	ΔE_{vdw}	ΔG_{GB}	$\Delta G_{nonpolar}$	electrostatic components ($\Delta G_{GB} + \Delta E_{elec}$)	nonpolar components ($\Delta G_{nonpolar} + \Delta E_{vdw}$)	ΔG_{tot}
7EMDCPT	−26	−71	48	−4	22	−75	−53
CPT	−20	−63	39	−4	19	−67	−47

[a] The standard error of mean <0.5 kcal mol^{-1}.

3.3. Biological Perspective. We used the flanking base pairs models to establish a mechanistic basis for the persistence of the ternary complexes. Our results indicate that the persistence of the ternary complexes correlate with (i) the calculated free-energy barrier for dissociation of the CPTs from the flanking base pairs, (ii) the ability of the CPTs to remain bound in the cleavage site during rotation of the flanking base pairs, (iii) the strength of the nonpolar interactions, and (iv) the stacking area between the CPTs and the flanking base pairs. We conceive that the nature and strength of the interactions between the CPTs and the flanking base pairs are important factors contributing to the persistence of the ternary complexes.

3.4. Drug Discovery Perspective. Rapid dissociation of the CPTs from the ternary complexes limits the clinical applications of some CPTs.[7] Extensive research efforts have been devoted to modification of existing drug leads in order to improve the persistence of the ternary complexes.[13,24] However, the large variance in the persistence of the ternary complexes is apparently neither explicable nor predictable.[12] According to our flanking base pairs models the CPTs that are capable of forming the most persistent ternary complexes share four characteristics: (i) higher ΔG_{PMF}; (ii) larger quadratic zones; (iii) higher $\Delta G_{nonpolar}$ and ΔE_{vdw} energies; and (iv) larger stacking areas with the flanking base pairs. Recently, Elban et al. measured off-rates for 10,11-MD-14-azaCPT (10,11-methylenedoxy-14-azacamptothecin) and 14-azaCPT (14-azacamptothecin).[13] Incorporation of the 10,11-MDO moiety into 14-azaCPT increased the persistence of the ternary complexes (Table 1). To further illustrate the potential application of our flanking base pairs models in the context of drug discovery, the 14-azaCPT/10,11-MDO-14-azaCPT-flanking base pairs models were calculated. As expected, the calculated free-energy barrier for dissociation of 14-azaCPT ($\Delta G_{PMF} = 7.7$ kcal mol^{-1}) from the flanking base pairs is lower than that of 10,11-MDO-14-azaCPT ($\Delta G_{PMF} = 9.2$ kcal mol^{-1}). 10,11-MDO-14-azaCPT (quadratic zone = 62°) is less sensitive to changes in the rotation angles of the flanking base pairs when compared with 14-azaCPT (quadratic zone = 50°). Incorporation of a 10,11-MDO moiety into 14-azaCPT leads to an increase in nonpolar energies ($\Delta G_{nonpolar} + \Delta E_{vdw}$, 10,11-MDO-14-azaCPT = −49 kcal mol^{-1} and 14-azaCPT = −44 kcal mol^{-1}). Furthermore, the stacking area of 10,11-MDO-14-azaCPT (98 Å^2) is larger than that of 14-azaCPT (93 Å^2). In brief summary, the results obtained using our flanking base pairs models demonstrate the power of using molecular dynamics approaches to estimate the persistence of the drug-induced ternary complexes during the lead optimization phase of the drug discovery process.

4. Conclusion

The low persistence of CPTs-induced ternary complexes currently limits clinical applications of many CPTs. In the present study, we performed molecular dynamic simulations for the CPTs-induced ternary complexes. In these ternary complexes models correlated motions between the CPTs and the flanking base pairs were found to be important. On the basis of our results we infer that the nature and strength of the bindings between the CPTs and the flanking base pairs may shed light on the factors underlying the significant variation in the persistence of the ternary complexes. Our 'flanking base pairs' models reveal that the CPTs that induce the most persistent ternary complexes share the following characteristics: (i) they dissociate less readily from the flanking base pairs; (ii) they are less sensitive to changes in the rotation angles of the flanking base pairs; (iii) they have higher nonpolar interaction energies with the flanking base pairs; and (iv) they have larger stacking areas with the flanking base pairs. Our results indicate that flanking base pairs models can be used to predict the persistence of the ternary complexes during the lead optimization stage of the drug discovery process, and MD simulations can be used to gain valuable insight into the mechanistic basis for the variation in the persistence of the ternary complexes.

Acknowledgment. This work was supported by the Areas of Excellence Scheme administered by the University Grants Committee of the Hong Kong Special Administrative Region, China (AoE/P-10/01). The small project funding granted to Fung-Ming Siu by the Committee on Research and Conference Grants (CRCR) and University Development Fund granted to Chi-Ming Che are gratefully acknowledged. We thank Dr. Rory Watt for his help editing this manuscript.

Supporting Information Available: Root-mean-square derivation of the 7EMDCPT-flanking base pair model; correlation between experimental half-lives of the CPTs measured by Holden et al. and Tanizawa et al.; PMFs of the 7EMDCPT-flanking base pairs model as a function of distance (χ) obtained under various conditions; PMFs of the 7EMDCPT-flanking base pairs model as a function of rotation angle (θ) obtained under various conditions; lactone and carboxylate forms of camptothecin. This material is available free of charge via the Internet at http://pubs.acs.org.

JA806934Y